

RESEARCH ARTICLE

Optimization and impact assessment of Aeolus HLOS wind assimilation in NOAA's global forecast system

Kevin Garrett¹  | Hui Liu^{1,2} | Kayo Ide³ | Ross N. Hoffman^{1,2}  | Katherine E. Lukens^{1,2}

¹NOAA/NESDIS/Center for Satellite Applications and Research (STAR), College Park, Maryland USA

²Cooperative Institute for Satellite Earth System Studies (CISESS), University of Maryland, College Park, Maryland USA

³University of Maryland, College Park, Maryland USA

Correspondence

Kevin Garrett, NOAA/NESDIS/STAR, 5830 University Research Ct, College Park, MD 20740, USA.

Email: kevin.garrett@noaa.gov

Funding information

NOAA/NESDIS/OPPA Technology Maturation Program, Grant/Award Numbers: NA14NES4320003, NA19NES4320002

Abstract

The European Space Agency Aeolus mission launched the first-of-its-kind space-borne Doppler wind lidar in August 2018. The Aeolus Level-2B (L2B) Horizontal Line-of-Sight (HLOS) wind observations are integrated into the NOAA Finite-Volume Cubed-Sphere Global Forecast System (FV3GFS). Components of the data assimilation system are optimized to increase the forecast impact from these Aeolus observations. Three observing-system experiments (OSEs) are performed using the Aeolus L2B HLOS winds for the period of August 2–September 16, 2019: a baseline experiment assimilating all observations that are operationally assimilated in NOAA's FV3GFS but without Aeolus; an experiment adding the Aeolus L2B HLOS winds on top of the baseline configuration; and an experiment adding the Aeolus L2B HLOS winds on top of the baseline but also including a total least-squares (TLS) regression bias correction applied to the HLOS winds. The variances of the Aeolus HLOS wind random errors (i.e., observation errors) are estimated using the Hollingsworth–Lonnberg (HL) method. Results from both OSEs demonstrate positive impact of Aeolus L2B HLOS winds on the NOAA global forecast. The largest impact is seen in the tropical upper troposphere and lower stratosphere where the Day 1–3 wind vector forecast root-mean-square error (RMSE) is reduced by up to 4%. Additionally, the assimilation of Aeolus impacts the steering currents ambient to tropical cyclones, resulting in a 15% reduction in track forecast error in the Eastern Pacific basin Day 2–5 forecasts, and a 5% and 20% reduction in track forecast error in the Atlantic basin at Day 2 and Day 5, respectively. In most cases, the additional TLS bias correction increases the positive impact of Aeolus data assimilation in the NOAA global numerical weather prediction (NWP) system when compared to the assimilation of Aeolus without bias correction.

KEYWORDS

Aeolus winds, bias correction, Doppler wind lidar, NWP impact

1 | INTRODUCTION

Atmospheric wind plays a critical role in weather and weather forecasting; from boundary-layer surface

interactions and mixing, to transport of moisture, aerosols, and atmospheric constituents, and influence on the formation and evolution of extreme weather events such as hurricanes and winter storms. Accurate representation

of the three-dimensional wind field at forecast initialization, through the assimilation of wind observations as well as other observations related to wind through conservative quantities or advection, is important for short- and medium-range forecast skill (e.g., Bengtsson *et al.*, 2005). Currently, the global observing system provides wind observations to operational National Oceanic and Atmospheric Administration (NOAA) global numerical weather prediction (NWP) from radiosonde, surface stations and ocean buoys, from aircraft, and from space including ocean surface vector winds from scatterometers, and Atmospheric Motion Vectors (AMVs) from geostationary and polar-orbiting infrared imagers and sounders (Kleist *et al.*, 2009; Bi *et al.*, 2011). Apart from wind profile observations from rawinsondes and aircraft near major airports, which have limited geographic coverage, these wind observations are confined to a horizontal plane, with minimal information about the variation of the wind in the vertical dimension. Recent studies have highlighted the gap in wind profile (3D-wind) observations, and the expected benefits both for NWP as well as boundary-layer physics understanding (Anthes *et al.* 2019, National Academies of Sciences, 2018). To address these gaps, Doppler wind lidar technology on a space-borne platform has been pursued to measure 3D-winds, and was realized with the Aeolus mission of the European Space Agency (ESA).

Aeolus was launched in August 2018, providing the first observations of wind profiles from a space-borne Doppler wind lidar (Stoffelen *et al.*, 2005; Reitebuch *et al.*, 2009; Reitebuch, 2012; Straume-Lindner, 2018). Aeolus measures both Rayleigh (i.e., molecular) and Mie (e.g., clouds and aerosols) backscatter to derive Horizontal Line-of-Sight (HLOS) wind profiles throughout the troposphere and lower stratosphere (Straume *et al.*, 2020). The Aeolus HLOS Level-2B (L2B) winds have been evaluated and assimilated in operational data assimilation systems at NWP centers worldwide and have demonstrated positive impact on global weather forecasts (Cress, 2020; Rennie *et al.*, 2021) but to date only neutral impacts have been reported for regional NWP (e.g., Hagelin *et al.*, 2021). As part of the Aeolus calibration and validation effort, as well as to support planning of the NOAA next-generation satellite architecture, the value of Aeolus observations on NOAA's mission to understand and predict changes in climate and weather has been investigated. The overall study includes the assessment of Aeolus data quality, the integration of Aeolus into NOAA regional and global NWP, and the ability of Aeolus observations to improve the use and impact of other observation types assimilated in NWP (e.g., AMVs). The present study focuses on the impact of Aeolus winds on global NWP, while other recent studies have focused on the quality and added value of Aeolus winds to

other observing systems (e.g., AMVs) (Hoffman *et al.*, 2022; Lukens *et al.*, 2022).

The approach to assimilating Aeolus data in NOAA global NWP, specifically the Finite-Volume Cubed-Sphere Global Forecast System (FV3GFS), including the random-error estimates of Aeolus winds, bias correction, and quality control, is given in Section 2. The impact of Aeolus winds on NOAA global forecasts including forecasts of tropical cyclone tracks are examined in Section 3. A summary of the findings and conclusions on the impact of Aeolus winds on NOAA global forecasts are presented in Section 4.

2 | METHODOLOGY

2.1 | Data and model

Throughout the lifetime of the Aeolus mission, various versions of the L2B dataset have been made available for evaluation and data assimilation impact studies. HLOS wind measurements are taken by the Atmospheric Laser Doppler Instrument (ALADIN) ultraviolet (UV) laser operating at 355 nm with receivers measuring both Rayleigh and Mie backscatter (Andersson *et al.*, 2008; Rennie *et al.*, 2020). The Rayleigh and Mie channels provide HLOS winds up to 30 km, with a vertical resolution between 250 m and 2 km, depending on the laser rangebin configuration.

HLOS wind L2B data from the Aeolus Flight Model A (FM-A) laser became available shortly after launch in September 2018, but the data experienced drifts in bias, and reductions in laser energy and signal to noise (Liu *et al.*, 2020; Reitebuch *et al.*, 2020; Weiler *et al.*, 2021). However, initial impact studies showed positive impact from Aeolus on global NWP (Rennie *et al.*, 2019; Garrett *et al.*, 2020). In June 2019, power was transferred to the FM-B laser in order to improve the wind data quality. The Aeolus Rayleigh-clear and Mie-cloudy winds (L2B10, de Kloe, 2019; de Kloe *et al.*, 2020) were downloaded from <https://earth.esa.int/eogateway/missions/aeolus> spanning the period of August 2–September 16, 2019 for this study, as recommended by ESA. One major correction applied to the Aeolus L2B winds by ESA is the M1 bias correction, which removes systematic errors due to earth-shine in certain orbit locations, affecting the telescope mirror temperature stability. The M1 correction combines European Centre for Medium-range Weather Forecasts (ECMWF) forecast information with temperature readings across the Aeolus M1 telescope mirror to predict the Aeolus wind bias (Weiler *et al.*, 2021).

The Aeolus L2B data are integrated and assimilated into the FV3GFS v15.3 global forecast model with the FV3GFS v16 physics package (Kleist *et al.*, 2021). The FV3GFS data assimilation system, or Global Statistical Interpolation (GSI, Kleist *et al.*, 2009) used in this study employs the 4DVar algorithm at C384 (25 km for the deterministic analysis and forecast) and C192 (50 km for the 80 ensemble members) horizontal resolution, with 64 vertical levels (Wang and Lei, 2014). The FV3GFS background winds are interpolated to the three-dimensional location (latitude, longitude, and height) and time of each Aeolus wind observation and transformed to the HLOS wind background equivalent ($HLOS^b$) using

$$HLOS^b = -u \sin(\varphi) - v \cos(\varphi) \quad (1)$$

where u is the zonal wind component, v is the meridional wind component, and φ is the satellite azimuth angle of the HLOS measurement. The Aeolus winds are assimilated as a function of height in the NOAA data assimilation system. Considering the horizontal resolution (25 km) of the FV3GFS model used in this study, the Mie winds were thinned along track to 90 km horizontal resolution. In future experiments we may explore the benefit of thinning Mie winds at higher resolutions on GFS forecasts.

In what follows, the Aeolus observed and FV3GFS-equivalent HLOS winds are referred to as Aeolus and FV3GFS winds, respectively. In the discussion of winds that are not HLOS winds, terms such as u -wind, v -wind, or wind vector are used.

2.2 | Random-error estimates of Aeolus winds

Although other studies mentioned previously have focused on assessing Aeolus data quality using multiple wind references (aircraft, AMV, rawinsonde, etc.), the characterization of random and systematic errors of Aeolus winds relative to the FV3GFS 6-hr forecast (i.e., background) are critical for optimizing the impact of Aeolus winds on NOAA FV3GFS forecasts. In general, data assimilation systems require proper estimation of the error characteristics of the input data sources such as the background and observations. Any known, large systematic errors (hereafter biases) should be removed, and the standard deviation (SD) of the observation random errors including instrument and representativeness errors should be accounted for. In this study, the Hollingsworth–Lonnberg (HL) method (Hollingsworth and Lonnberg, 1986) is applied to the sum of these random errors to determine Aeolus observation errors by analyzing the spatial correlation structure from the random component of differences

between the Aeolus winds and FV3GFS background winds. It is assumed that there are no correlations between the random errors of the Aeolus and FV3GFS winds, and no horizontal correlations between the random errors of Aeolus winds separated by more than 90 km. It is noted that Rayleigh winds are the result of averaging along a 90-km accumulation length. As such, some error correlations between adjacent Rayleigh winds would be expected at the distance of 90 km. Typically, Mie winds are the result of averaging along a 15-km accumulation length and are therefore less sensitive to error correlations at 90-km separations. However, the impact of potential correlation at 90 km distance on the error estimate is excluded, as indicated in Equation (3) below. These assumptions are justified *a posteriori* by the reasonable error estimate of FV3GFS background winds as shown below.

The error estimates are calculated for all Aeolus winds in each layer as follows. The layer centers are defined by the global average height of the Rayleigh and Mie winds in each vertical range-bin. First, the spatial variance of Aeolus observation minus background (O–B) is calculated, where Aeolus data are not assimilated. Under the assumption that the Aeolus and FV3GFS background errors are uncorrelated, the covariance of O–B, $(\sigma^{o-b})^2$, is equal to the sum of the variance of the random error of Aeolus winds and FV3GFS winds,

$$(\sigma^{o-b})^2 = (\sigma^o)^2 + (\sigma^b)^2 \quad (2)$$

where σ^o and σ^b are the random error standard deviations of Aeolus winds and FV3GFS background winds, respectively.

By assumption, at separation distances greater than 90 km, the O–B covariances are estimates of the FV3GFS error covariance alone and can be extrapolated back to zero separation to get an estimate of the error variance of the FV3GFS winds, $(\sigma^b)^2$, and then, using Equation (1), the error variance of the Aeolus winds, $(\sigma^o)^2$, may be determined. Note that this can only be done when using O–B covariances at separation distances large enough to have negligible covariances between the Aeolus winds.

Specifically, the sample covariance is calculated from all innovation pairs with separation distances that fall within each bin; the bins are centered from 90 to 990 km with a width of 90 km, (e.g., the first bin is from 45 to 135 km). The sample covariance R is fit to the following function (similar to Bormann *et al.*, 2003) using unweighted least squares:

$$R_n = (\sigma^b)^2 (1 + r_n/L) \exp^{-r_n/L} \quad (n = 2, N) \quad (3)$$

Here L is the FV3GFS background covariance length scale, n is the bin index (note that bin 1 is

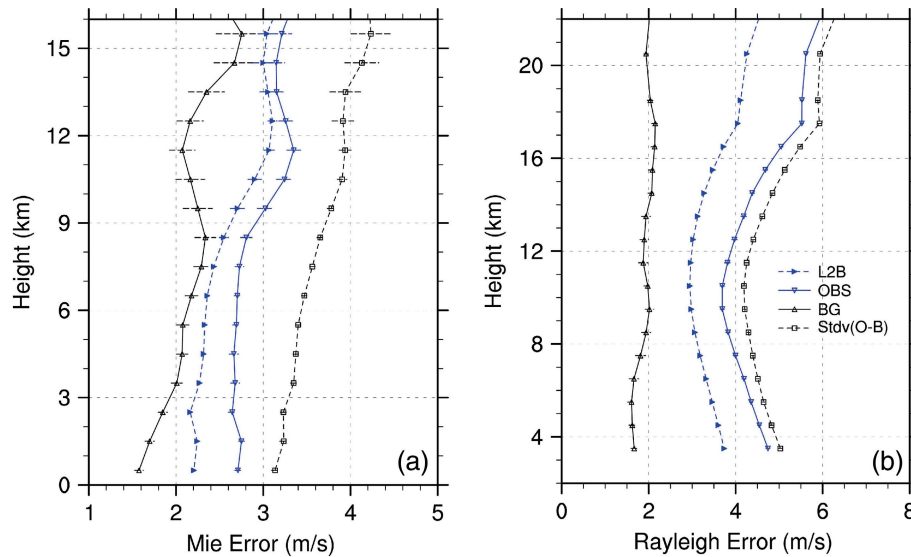


FIGURE 1 Vertical distributions of the random errors (m/s) of Aeolus (a) Mie and (b) Rayleigh winds estimated from all Aeolus minus FV3GFS background winds in each layer using the Hollingsworth–Lonnberg (HL) method (solid green line). Also shown, for the same sample, are the standard deviation of Aeolus minus FV3GFS background winds (dashed black line), the HL estimate of the FV3GFS background wind error (solid gray line), and the L2B estimated observation error (dashed blue line). The period covered is August 2–September 16, 2019

ignored to exclude impact of potential correlations at 90 km separation distance on the least-squares fit), r is the average separation distance in bin n , and N is the total number of bins, 11. See Hollingsworth and Lonnberg (1986) for further details.

Residual biases in the Aeolus wind O–B innovations may introduce small spurious correlations (0–0.09). To reduce the impact of the biases, spurious correlation at the separation distance of 1,000 km is considered due to the biases and is removed from the correlations at all separation distances before the fitting to Equation (3).

Figure 1 shows the random-error estimates in the Aeolus and FV3GFS background winds calculated for August 2–September 16, 2019. The FV3GFS wind error estimates are ~ 2 m/s, which is consistent with typical estimates of u - and v -wind background error SD (Rennie *et al.*, 2021). The Mie and Rayleigh wind error estimates are larger, about 2.5–3.4 m/s and 3.8–6.0 m/s, respectively, and the Rayleigh wind errors are comparable to errors of AMVs assimilated in the NOAA global data assimilation system (Jung *et al.*, 2016). Note that the HL Aeolus error estimates have very similar vertical distributions to the O–B innovation SD and the L2B estimated uncertainty, but the L2B uncertainty may be underestimated, particularly for Rayleigh winds. The HL estimate of the Aeolus wind errors shown in Figure 1 are used in the analyses of this study.

2.3 | The TLS bias correction

Variational data assimilation minimizes a cost function and theoretically requires that the observations and the NWP state are unbiased. Existence of any such biases may

make the analysis sub-optimal (Daley, 1991). To optimize the impact of Aeolus winds on NWP, any biases between Aeolus winds and NWP model background winds should be removed.

Assessing systematic errors after the M1-correction, Liu *et al.* (2022) showed that residual biases exist between the Aeolus Rayleigh and Mie winds and FV3GFS background winds, and that these biases vary by latitude, height, and wind speed. Therefore, Liu *et al.* propose an additional bias correction for Aeolus wind innovations, that is, for O–B. The bias correction is based on a total-least-squares (TLS) regression analysis of the biases between Aeolus and FV3GFS background winds. For each assimilation cycle, the coefficients are calculated using the Aeolus and FV3GFS winds from the week before the current cycle, that is, from the previous 28 cycles. To consider the dependence of the bias on latitude, height, and orbit phase (ascending or descending), the coefficients are computed for 19 discrete bins of latitude (centered every 10° between 90°S to 90°N) and in each layer for ascending and descending orbits, separately. The coefficients are linearly interpolated to the latitude of each innovation. The calculated TLS estimated biases are then subtracted from each Aeolus wind innovation before assimilation. Figure 2 shows the zonal mean Rayleigh minus FV3GFS background winds before and after the TLS bias correction. Even with the M1 correction applied residual biases exist: up to -0.9 m/s in the ascending orbit lower troposphere, and up to 1.8 m/s in the descending orbit tropical upper troposphere/lower stratosphere regions. The biases are largely removed by the TLS bias correction. The large speed-dependent biases in Mie winds minus FV3GFS winds are also removed by the TLS bias correction (see Liu *et al.*, 2022).

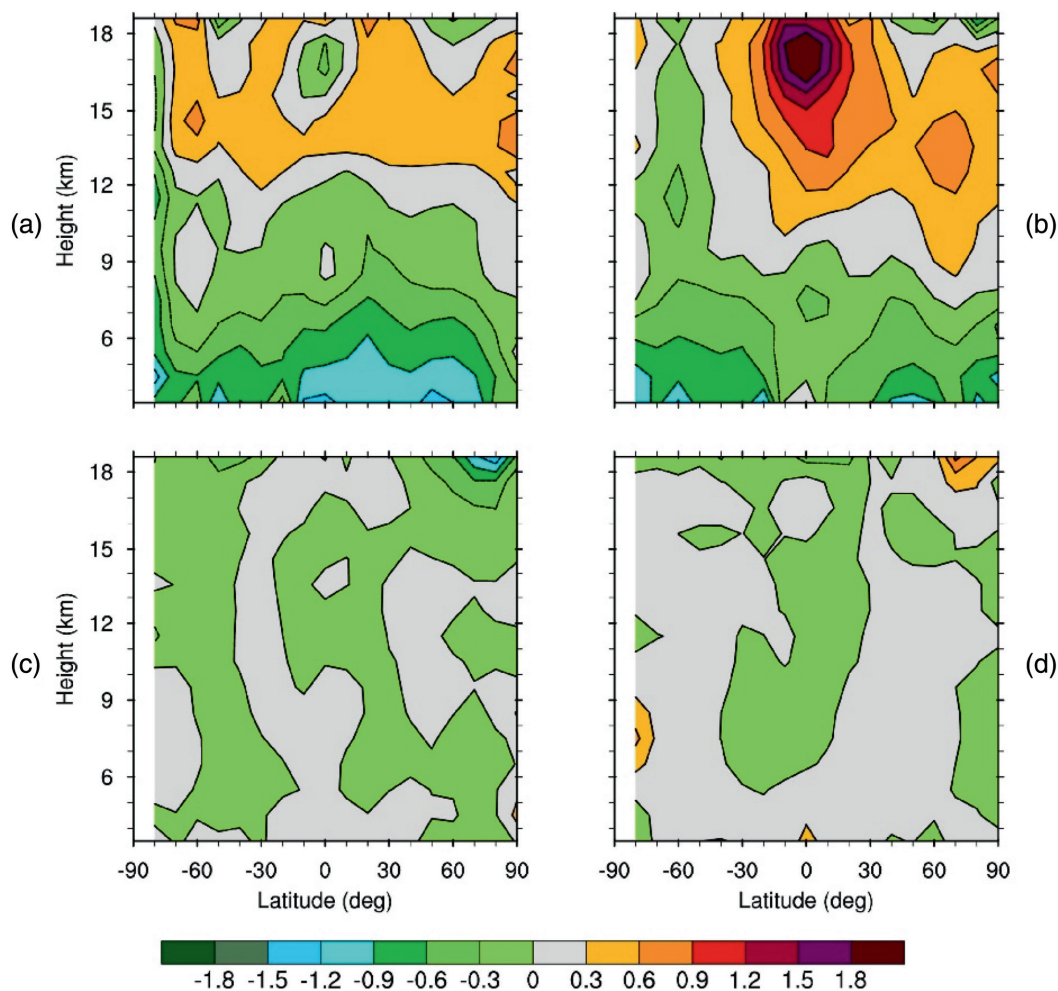


FIGURE 2 Latitudinal and height distributions of the mean difference (m/s) for Rayleigh minus FV3GFS winds from September 1–7, 2019 before (top row: a, b) and after (bottom row: c, d) applying the total least-squares (TLS) bias correction in ascending (left column: a, c) and descending (right column: b, d) orbits

2.4 | Experiments and quality control

To assess the benefits of assimilating Aeolus HLOS winds in the NOAA FV3GFS, three observing-system experiments (OSEs) are performed: the baseline experiment (BASE) without the assimilation of Aeolus winds; the experiment AEOM which assimilates the Aeolus winds; and AEOT which assimilates the Aeolus winds with the additional TLS bias correction. The three OSEs each assimilate all satellite and conventional observations routinely assimilated in NOAA operations.

Similar Aeolus data quality control procedures as recommended by ESA and ECMWF (Rennie *et al.*, 2021) were implemented to reject the following observations: HLOS L2B confidence flag “invalid”; HLOS Rayleigh winds at layers below 850 hPa, L2B uncertainties greater than 12 m/s, accumulation lengths less than 60 km, and atmospheric pressure within 20 hPa of topographic surface pressure; Mie HLOS winds with L2B uncertainties greater

than 5 m/s and accumulation lengths less than 5 km. A standard gross-check on the O–B (greater than four times the prescribed Aeolus wind errors shown in Figure 1) is also applied in the assimilation system.

3 | OSE RESULTS

3.1 | Global analysis and forecast impact assessment

The systematic adjustment to the analysis by the Aeolus winds is illustrated in Figure 3 by the mean differences between the experiment analyses and the BASE analysis. The difference between AEOM and BASE shows an evident impact in the u -wind in the troposphere and lower stratosphere around the equator, with the largest decrease in the mean analysis u -wind exceeding 0.5 m/s around 100 hPa. On the other hand, the mean analysis difference

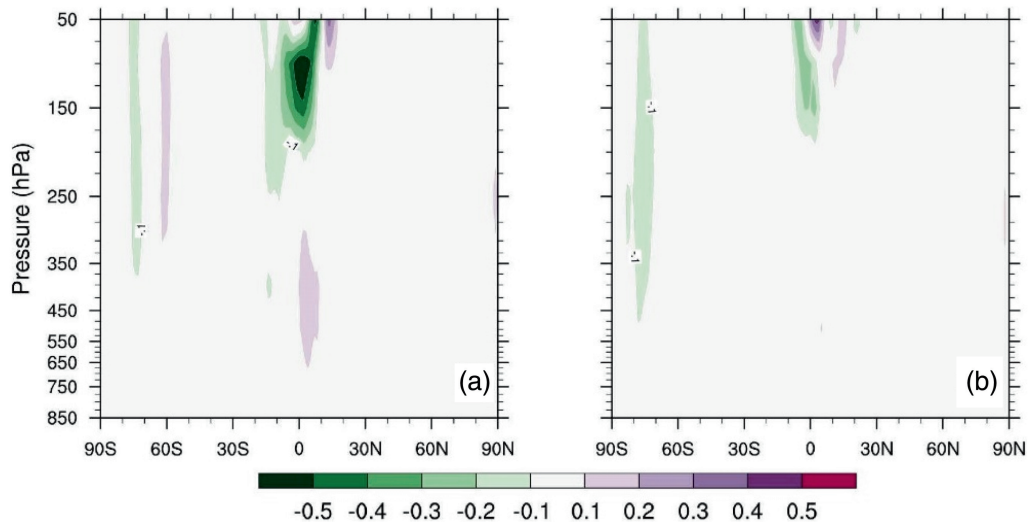


FIGURE 3 Zonal mean of analysis differences in u -wind (m/s) for (a) AEOM – BASE, and (b) AEOT – BASE, for the period of August 2–September 16, 2019. The latitudinal bins are centered from 90°S to 90°N every 10°

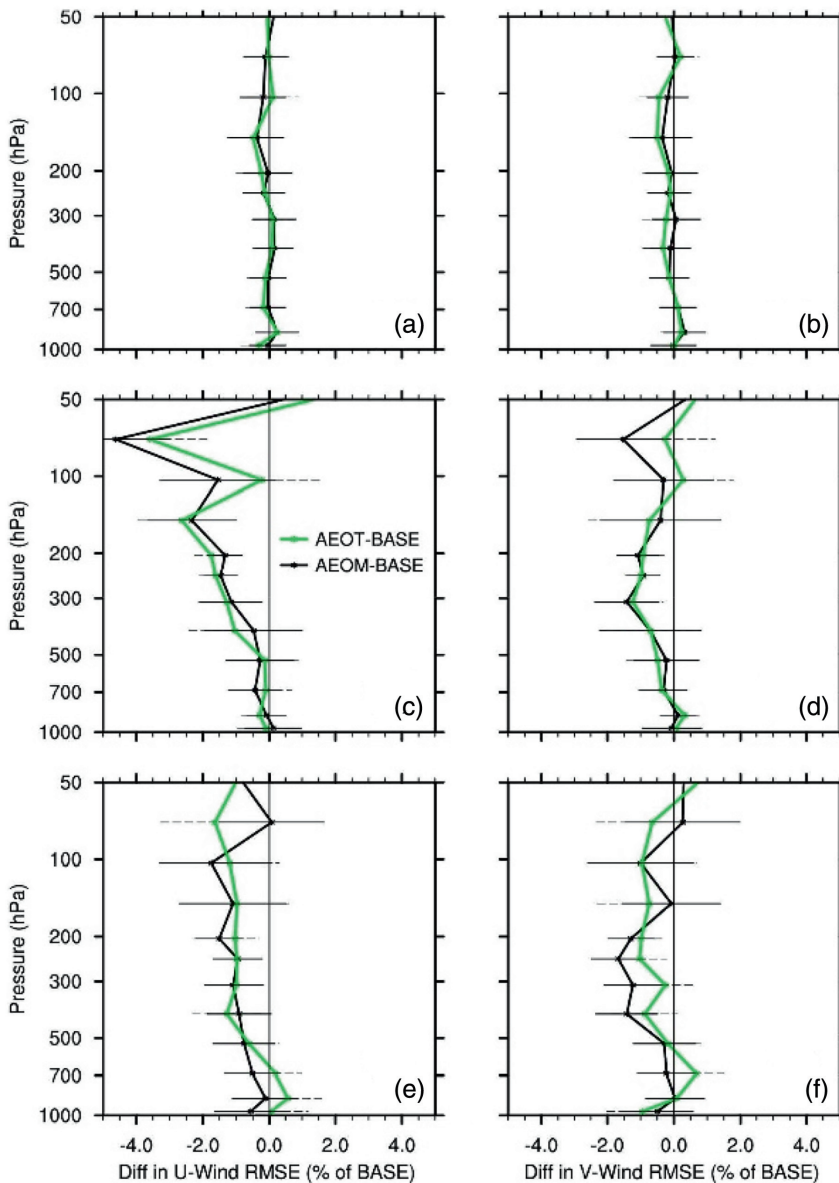


FIGURE 4 Profiles of mean observation minus FV3GFS 6-hr forecast background (O–B) root-mean-square (RMS) differences (%) for rawinsonde and aircraft u -wind (column, a, c, e) and v -wind (column, b, d, f). RMS differences for AEOM minus BASE (black lines) and AEOT minus BASE (green lines) are shown in the Northern hemisphere (top, a, b), tropics (middle, c, d), and Southern hemisphere (bottom, e, f). Horizontal bars denote the confidence interval at the 95% level in each layer. The period covered is August 2–September 16, 2019. Negative values imply an improvement due to the addition of Aeolus observations

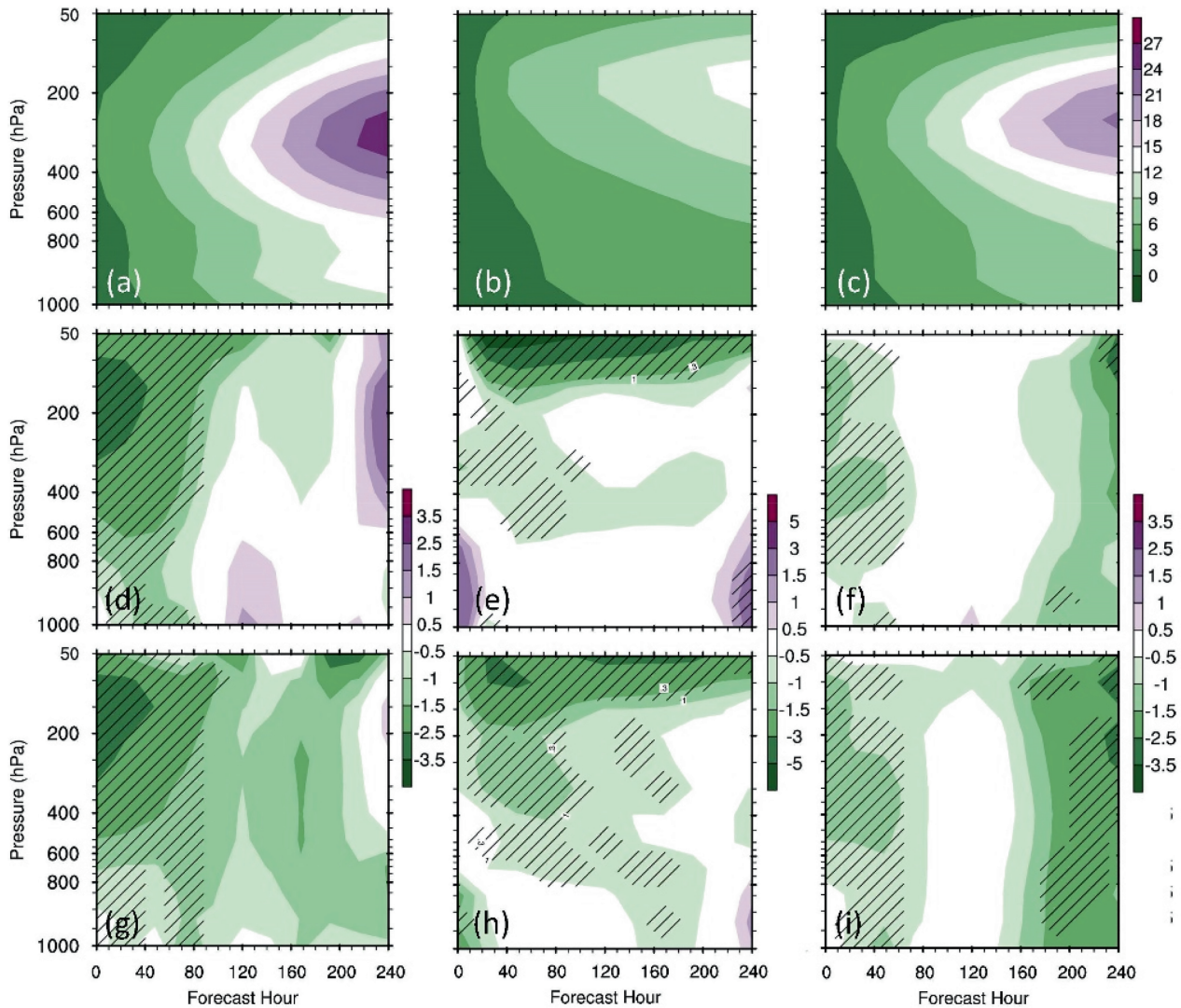


FIGURE 5 Vertical cross-sections of wind vector forecast root-mean-square error (RMSE) versus forecast hour (verified against European Centre for Medium-range Weather Forecasts [ECMWF] analysis) in the BASE experiment (top, a, b, c, m/s) for the Southern hemisphere (left), tropics (center), and Northern hemisphere (right). The RMSE difference with respect to BASE (%) are shown for AEOM (middle, d, e, f) and AEOT (bottom, g, h, i). The hatched areas are changes with at least 95% statistical significance

between AEOT and BASE shows a much-reduced impact in the same region. The reduced impact is consistent with the TLS bias correction removal of residual biases in the Aeolus wind data, shown in Figure 2b. The mean analysis difference between AEOM and BASE near 60°S above 500 hPa is also reduced with AEOT. The results suggest that without the additional bias correction to the Aeolus data, the assimilation of the Aeolus observations may result in over-estimated wind analysis increments.

Note that for the easterly wind at the equator at about 16 km (100 hPa), Aeolus HLOS winds are negative for ascending and positive for descending orbits. The large positive bias in HLOS O–B in the descending orbit (Figure 2b) indicates stronger easterly flow observed by Aeolus than forecast by the FV3GFS model. This leads

to stronger easterlies in the AEOM analysis, and negative u -wind component AEOM–BASE analysis differences.

Figure 4 shows the differences in the root-mean-square error (RMSE) fit of the FV3GFS u - and v -wind background (i.e., 6-hr forecasts) to conventional wind observations from rawinsonde and aircraft (O–B). Note that the spatial coverage by the rawinsonde and aircraft wind observations is irregular in general and quite sparse over remote regions, including the tropical oceans and the Southern Hemisphere. Therefore, corresponding statistics from these samples should be considered representative of the geographic coverage of the rawinsonde and aircraft observations only. Similar improvements in the RMSE fits for both AEOM and AEOT experiments are evident in the Southern Hemisphere and tropics u -wind. The largest

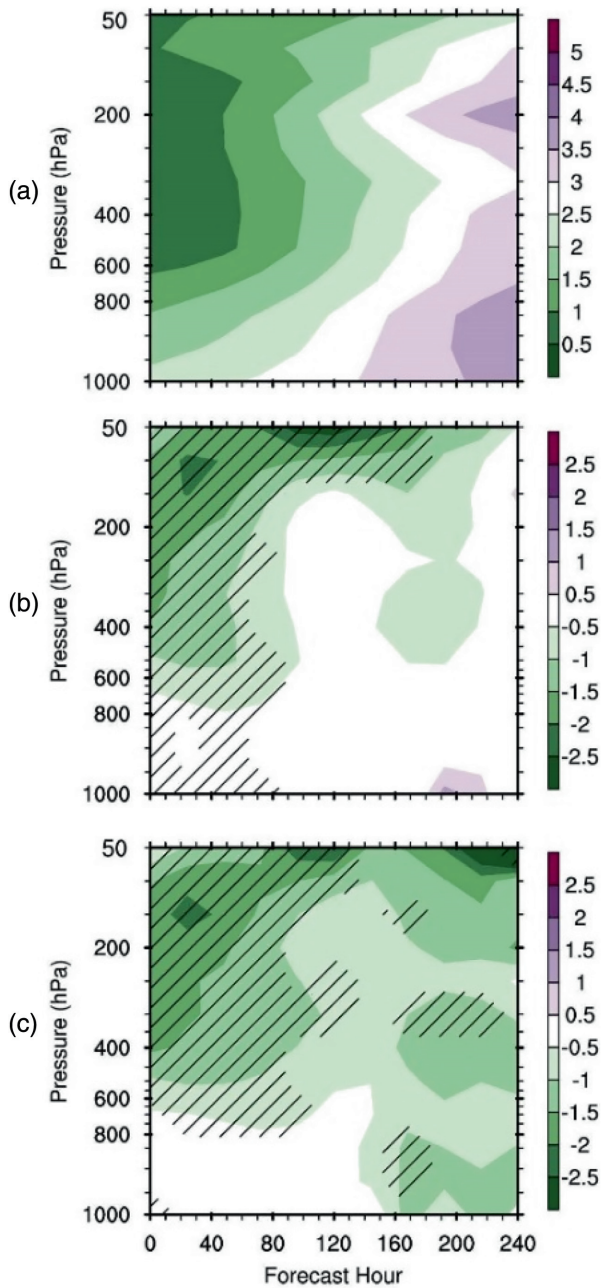


FIGURE 6 Vertical cross-sections of global temperature root-mean-square error (RMSE) versus forecast hour in (a) the BASE experiment (K), as well as the RMSE difference with respect to BASE (%) for (b) AEOM and (c) AEOT. As in Figure 5

reduction in RMSE for the u -wind occurs around 70 hPa in the tropics, which is about 4% reduction relative to the BASE RMSE. The RMSE is reduced in the Southern Hemisphere up to 1.5% throughout the mid-troposphere. More modest improvement of around 1% in RMSE is shown in the Southern Hemisphere and tropics for the v -wind at 200–300 hPa. It is noted that impact of the bias correction on the RMSE values for O–B of conventional winds is neutral in all regions. This could be partly related

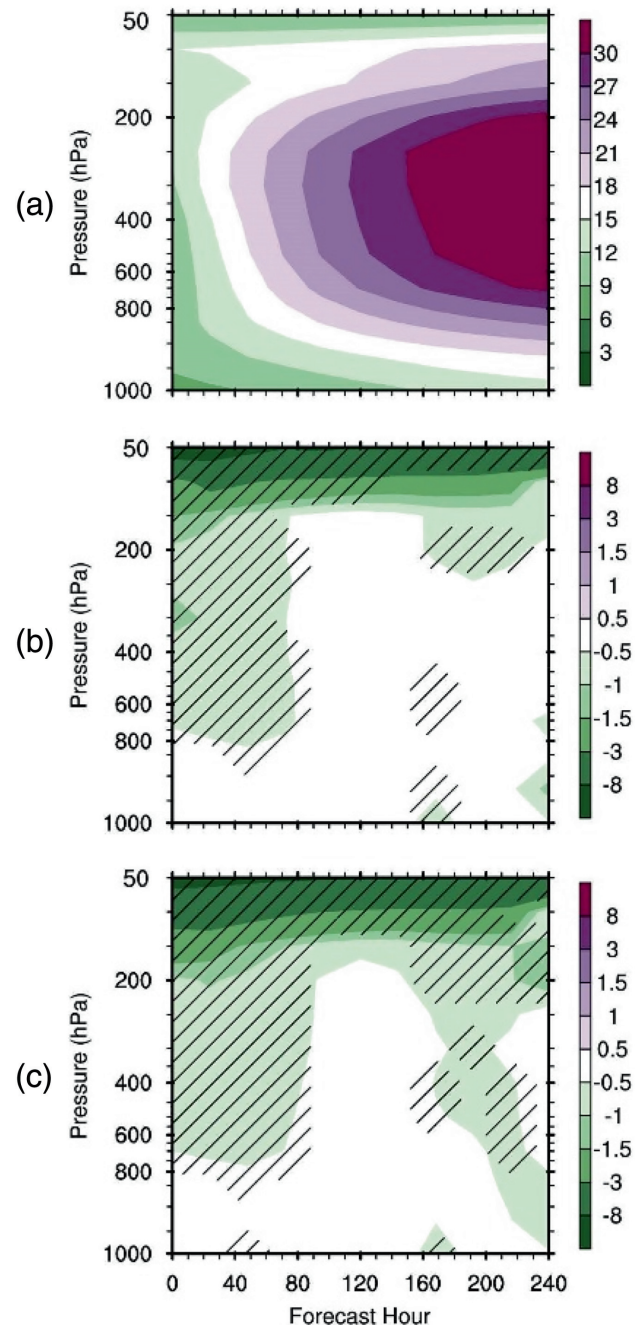


FIGURE 7 Vertical cross-sections of global relative humidity root-mean-square error (RMSE) versus forecast hour in (a) the BASE experiment (%), and the differences in RMSEs with respect to BASE (%) for (b) AEOM and (c) AEOT. As in Figure 5

to the fact that the conventional wind observations are sparse and limited to specific geographic areas within the tropics, whereas the bias correction is based on Aeolus minus FV3GFS background winds across the entire tropics. The RMSE is not noticeably reduced in the Northern Hemisphere, and this is expected due to the dense coverage of rawinsonde, aircraft, and other in situ data types that strongly impact the analyses.

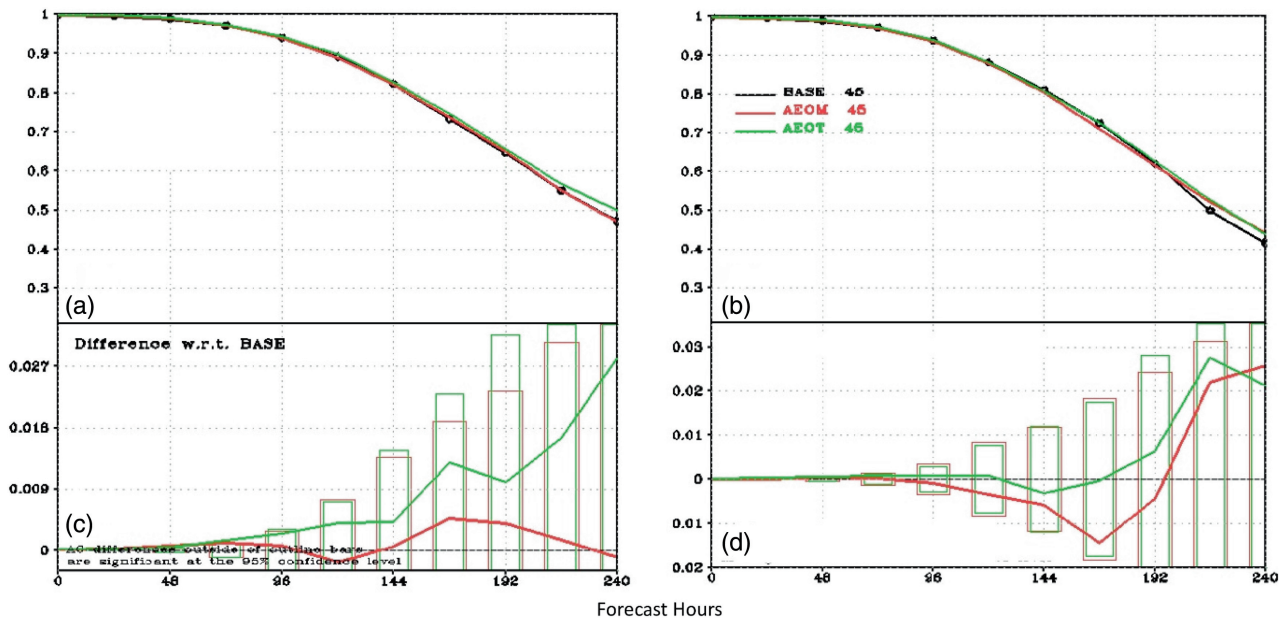


FIGURE 8 Anomaly correlation (AC, top panel) of FV3GFS 0- to 10-day 500 hPa height forecasts (verified against European Centre for Medium-range Weather Forecasts [ECMWF] analysis) in the BASE, AEOM, and AEOT experiments for (a, c) Southern and (b, d) Northern hemisphere. The differences in the ACs of AEOM and AEOT versus BASE are shown in the bottom panel, with bars representing the 95% confidence interval

The wind vector forecast RMSE from 50 to 1,000 hPa for Day 1–10 in BASE, verified against the ECMWF analysis, for the Southern Hemisphere, tropics, and Northern Hemisphere regions is shown in Figure 5. The differences in wind vector forecast RMSE between AEOM and BASE, and between AEOT and BASE are also shown. In general, the Aeolus impact on RMSE is positive in AEOM, with the largest error reduction (4%) seen above 100 hPa in the tropics and about 2.5% in the Southern and Northern Hemisphere. However, some minor degradation is seen in the tropics and the Southern Hemisphere, particularly at longer lead times. In AEOT, larger positive impacts are seen particularly in the troposphere and lower stratosphere in each region, at all forecast lead times. The degradations in AEOM are completely removed and turn to improvements in AEOT. The error reduction is increased from less than 1% to about 1.5% at longer forecast lead times at all levels in the Northern Hemisphere in AEOT. A large part of the improvement is statistically significant at the 95% significance level.

Figure 6 shows the BASE temperature forecast RMSE and differences for AEOM and AEOT, averaged globally. Aeolus winds have a positive impact on the temperature forecast. The RMSE is reduced by up to 1% in the troposphere and about 2.5% in the lower stratosphere at short-range forecast times in AEOM. In AEOT, the RMSE is further reduced in the troposphere at short-range forecast times and is also improved at longer forecast times compared with AEOM. The maximum RMSE reduction

reaches about 2.5% in the lower stratosphere and about 1% in the troposphere.

Furthermore, Aeolus winds substantially reduce the relative humidity forecast RMSE in AEOM compared to BASE (Figure 7). The RMSE is reduced up to 8% above 200 hPa for all forecast lead times, and about -0.5% , in the troposphere at short lead times. In AEOT, the positive impact is slightly improved at longer lead times. The improved RH forecast in the upper troposphere/lower stratosphere is likely related to the improved wind analysis as demonstrated in tropical regions, where temperature sounders have less impact on the upper-level wind fields compared with extratropical regions which are highly constrained by geostrophic balance. It should also be noted however, that there remains high uncertainty in the analysis of humidity in these regions due to many factors including the low volume of humidity observations and their higher uncertainty due to the overall low absolute humidity.

Impacts on the 500-hPa-height Anomaly Correlation (AC) in the Northern Hemisphere for both AEOM and AEOT are neutral, while some positive (not statistically significant) improvement is shown after Day 4 in the Southern Hemisphere in AEOT, compared to more neutral impacts for AEOM (Figure 8).

The forecast skill scorecards for AEOM and AEOT versus BASE (Figure 9) provide a comprehensive evaluation of the global forecast skill out to 10 days in terms of RMSE and AC. The Aeolus winds have statistically

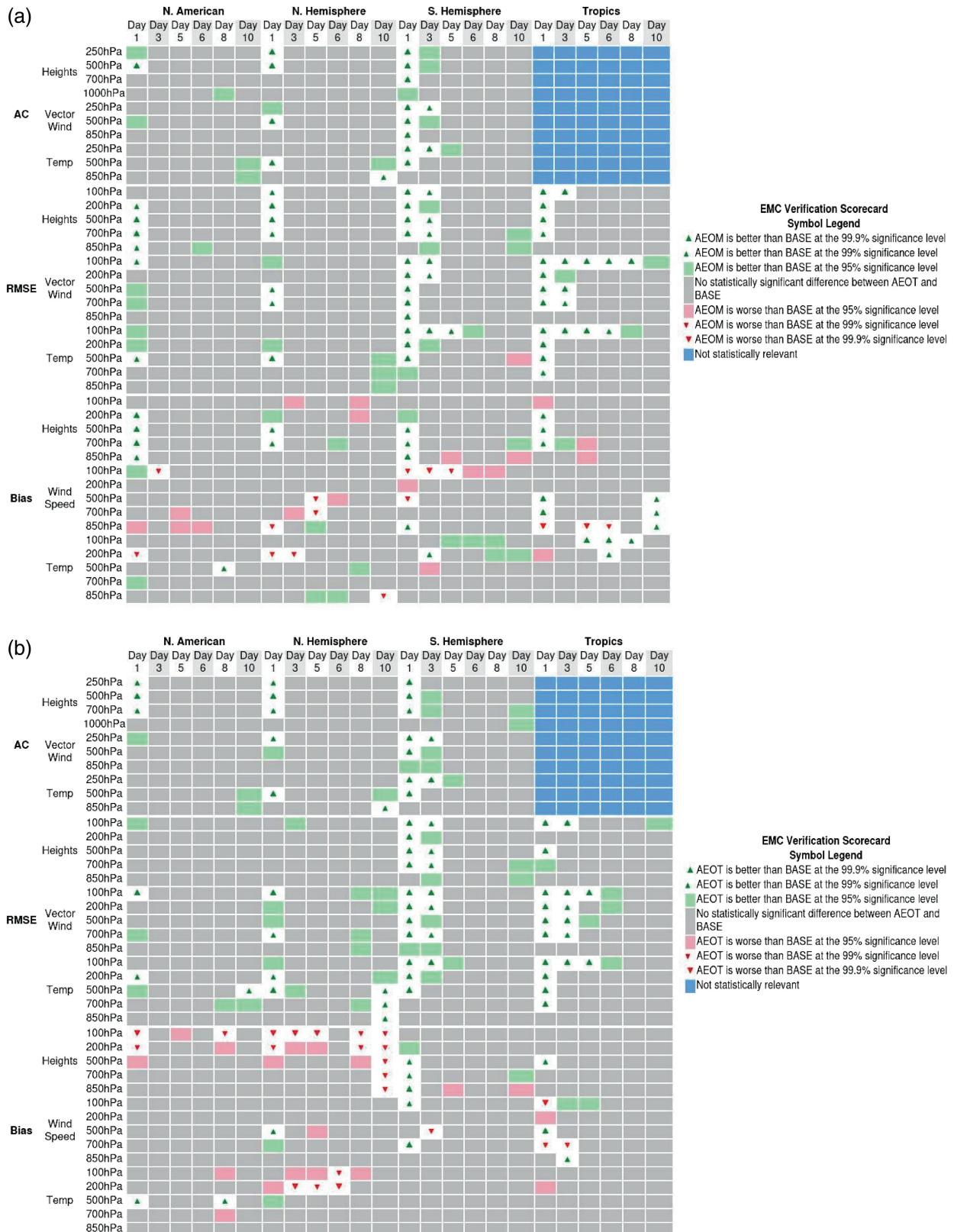
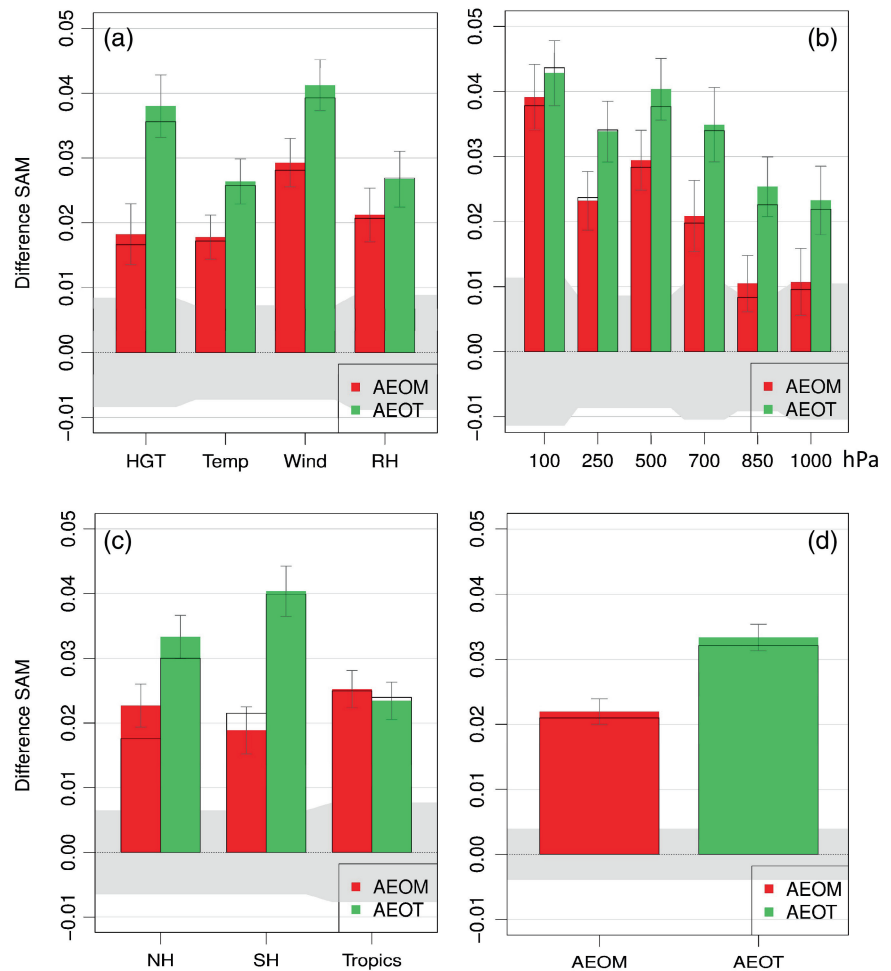


FIGURE 9 NOAA/NCEP 1- to 10-day global forecast skill scorecard for the FV3GFS forecasts comparing (a) AEOM versus BASE, and (b) AEOT versus BASE. European Centre for Medium-range Weather Forecasts (ECMWF) analysis is used in the verification. The symbol legend is shown above the panels

FIGURE 10 The difference summary assessment metric (SAM) overall forecast scores for AEOM, and AEOT versus BASE experiments. The scores are shown for (a) forecast parameters of temperature (temp), geopotential height (HGT), vector-wind (wind) and relative humidity (RH), (b) vertical levels, (c) geographic regions, and (d) overall performance of AEOM and AEOT. The gray areas indicate the 95% confidence level under the null hypothesis that there is no difference between experiments for this metric. In addition, the estimated uncertainty at the 95% level is indicated by small error bars at the ends of the color bars. Two normalizations are used, the empirical cumulative density function (ECDF, colors) and rescaled-minmax normalization (black outline). Details can be found in Hoffman *et al.* (2018). A value of 0.03, for example, indicates the average normalized statistic over all metrics is better (greater) by 0.03 than BASE. Under the null hypothesis that there are no differences, all SAMs would be 0.5, so a 0.03 improvement can be considered a 6% improvement (0.03/0.5) in normalized scores. NH, Northern hemisphere; SH, Southern hemisphere



significant positive impacts on forecast skill for wind and temperature in the tropics and the Southern Hemisphere in AEOM, for Days 1–3, but less positive impacts in the Northern Hemisphere and in North America. In AEOT, the application of the TLS bias correction leads to further improvement in both number of metrics and magnitude in all regions, for example more significant improvement is seen in wind and temperature forecasts throughout the troposphere from Days 1–10 in the Southern Hemisphere.

To quantify the scorecard results overall, the Summary Assessment Metric (SAM) is computed for the BASE, AEOM and AEOT experiments. The SAM illustrates the overall forecast skill by normalizing the AC and RMSE values for all experiments, parameters, levels, and lead times with respect to the computed empirical cumulative density function (ECDF) (Hoffman *et al.*, 2018). Assuming a null hypothesis that the mean of the ECDF for all experiments is 0.5, positive or negative impact on forecast skill can be determined for each forecast experiment depending on whether the null hypothesis is rejected and the mean is higher (positive impact) or lower (negative impact) than 0.5. Figure 10 shows the difference in SAM scores for AEOM and AEOT with respect to BASE separately for each

parameter (temperature, geopotential height, wind, and relative humidity), each vertical level, and each region, as well as the overall difference. Values above 0.0 demonstrate an increase in the mean of the normalized scores and improvement of the forecast versus the BASE, while the gray-shaded region represents the 95% significance level. Aeolus winds in general have a positive impact on the forecast of wind, temperature, height, and relative humidity at all vertical levels and for all the regions, with the largest impacts in the Southern Hemisphere for the AEOT experiment. The overall improvement by Aeolus winds for AEOM and AEOT is about 4% and 6.5%, respectively (Figure 10d), illustrating the increased forecast skill with the TLS bias correction.

3.2 | Tropical cyclone forecast impact assessment

The impact of Aeolus HLOS wind assimilation on tropical cyclone (TC) forecasts in the Eastern Pacific (EP) and Atlantic (AL) basins is assessed using the TC best track data from the NOAA National Hurricane

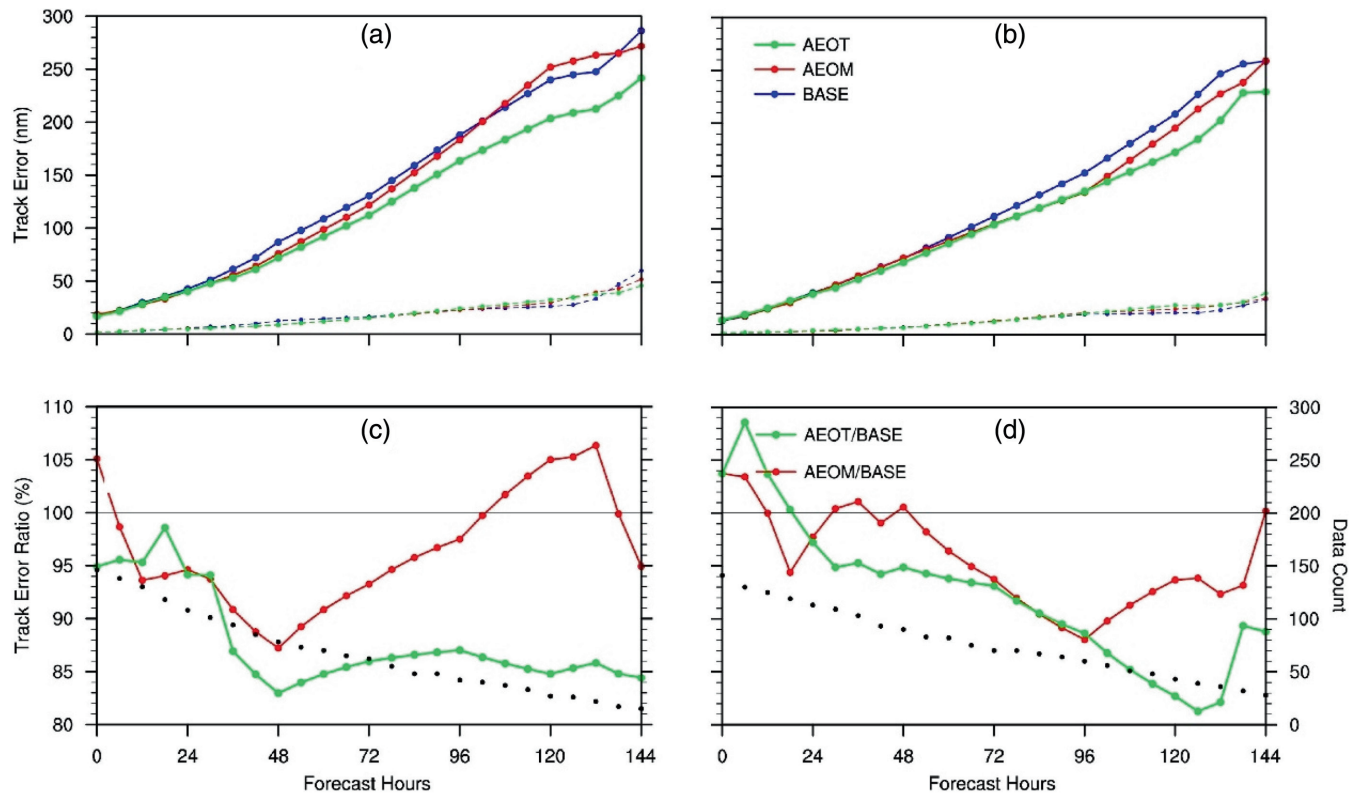


FIGURE 11 Means (solid lines) and confidence intervals (full width) at the 95% significance level (dashed lines) of FV3GFS Day-0–6 track forecast errors (top, a, b) in nautical miles (nm), and the track error ratios relative to BASE (bottom, c, d) of tropical cyclones in the eastern Pacific (left, a, c) and Atlantic (right, b, d) basins during the experiment period from BASE, AEOM, and AEOT. The black dots in the lower panels show the number of cases (right axis). The cyclones assessed include *Flossie*, *Gil*, *Henriette*, *Ivo*, *Juliette*, *Akoni*, *Kiko*, *Mario*, and *Lorena* in the eastern Pacific basin, and *Dorian*, *Erin*, *Fernand*, *Gabrielle*, *Humberto*, *Jerry*, *Imelda*, *Karen*, and *Lorenzo* in the Atlantic basin

Center (NHC) (<https://www.nhc.noaa.gov/data/>). During the experiment period, there were 18 named TCs. The average errors in the forecasts of TC track are shown in Figure 11. Aeolus impact on TC track forecast errors is mixed in the EP basin and positive after Day 2 in the AL basin in AEOM, compared to BASE. In AEOT, the track forecast errors are noticeably reduced in both basins. For example, the track error is reduced by about 15% in the EP basin and by ~5% to 15% in the AL basin after Day 2. The track improvements are marginally statistically significant at the 95% level for AEOT. Although the results are encouraging, more TC cases are needed to achieve more robust conclusions about Aeolus impact on TC forecast track.

4 | SUMMARY AND CONCLUSIONS

In this study, the impact of the Aeolus L2B10 HLOS winds assimilation into NOAA's global data assimilation system for the FV3GFS is assessed for the period of August 2–September 16, 2019. The random errors or weighting of Aeolus winds are estimated by the HL method and suggest

that the L2B HLOS wind uncertainty underestimates Aeolus observation errors. Since vertical profiles of HL error estimates have the same shape, but larger amplitude compared to the L2B estimated errors, it may be useful to scale the L2B errors for use in data assimilation systems. Two impact experiments were performed: the first using the M1-corrected L2B HLOS wind data, and the second applying additional bias correction based on the TLS regression approach. The experiments' forecasts were verified against ECMWF analyses, and the forecast skill was compared to the performance of a baseline experiment which assimilated all observations operationally assimilated at NOAA but not the Aeolus winds.

The results from the OSEs demonstrate that the Aeolus winds improve NOAA global forecast skill in terms of (1) 6-hr forecast verified against conventional wind observations from rawinsondes and aircrafts; (2) the Day 1–10 forecasts verified against ECMWF analyses; and (3) the forecast of TC track in the Eastern Pacific and Atlantic basins verified against NOAA/NHC best track data. The most prominent impacts are seen in the tropical upper troposphere/lower stratosphere wind forecast, and Southern

Hemisphere wind, temperature and height forecasts. Up to a 4% reduction in wind vector forecast RMSE is seen from 50 to 100 hPa, in both regions. Forecast impact in the Northern Hemisphere forecast is positive with a smaller magnitude. The assimilation of Aeolus reduces the TC track forecast error by 5%–20%, with the largest reduction occurring in the Day-5 forecast. It is worth highlighting that although the ESA M1 correction to the Aeolus HLOS data dramatically improves Aeolus L2B data quality, the forecast skill is considerably improved after applying the additional TLS bias correction. It is noted that a longer period and other seasons could be used in future experiments to obtain more statistically robust results.

The Aeolus mission is helping to address the 3D-winds gap in the satellite global observing system. Although the Aeolus HLOS wind observations are not operationally assimilated at NOAA, the assessment provides critical results for understanding the value and impact of Doppler wind lidar data on NOAA's global forecasts, and will accelerate the exploitation of any future lidar wind observations from space.

AUTHOR CONTRIBUTIONS


Kevin Garrett: Conceptualization; data curation; funding acquisition; methodology; project administration; writing – original draft; writing – review and editing. **Hui Liu:** Conceptualization; data curation; formal analysis; investigation; methodology; software; visualization; writing – original draft. **Kayo Ide:** Conceptualization; supervision; writing – review and editing. **Ross Hoffman:** Conceptualization; writing – review and editing. **Katherine E. Lukens:** Data curation; project administration; writing – review and editing.

ACKNOWLEDGMENTS

This work was supported by the National Oceanic and Atmospheric Administration/NESDIS Office of Projects, Planning, and Acquisition (OPPA) Technology Maturation Program (TMP) through CICS and CISESS at the University of Maryland/ESSIC (NA14NES4320003 and NA19NES4320002) managed by Patricia Weir and Dr. Nai-Yu Wang. The authors would like to acknowledge Dr. Michael Rennie (ECMWF) and Dr. Lars Isaksen (KNMI) for their comments and suggestions on the assimilation of Aeolus observations, and Dr. William McCarty with NASA/GMAO for providing earlier versions of the GSI with Aeolus ingest and observation operator capability. The Aeolus L2B BUFR data were provided by ECMWF. The scientific results and conclusions, as well as any views or opinions expressed herein, are those of the author(s) and do not necessarily reflect those of NOAA or the U.S. Department of Commerce.

ORCID

Kevin Garrett  <https://orcid.org/0000-0002-7444-4363>

Ross N. Hoffman  <https://orcid.org/0000-0002-4962-9438>

REFERENCES

- Andersson, E., Dabas, A., Endemann, M., Ingmann, P., and Källén, E. (2008) 'ADM-Aeolus'. Noordwijk, The Netherlands. ESA Communication Production Office. Available at: <https://earth.esa.int/documents/10174/1590943/AEOL002.pdf> (Accessed May 23, 2021)
- Anthes, R. A., and Coauthors (2019) Developing priority observational requirements from space using multi-attribute utility theory. *Bulletin of the American Meteorological Society*, 100(9), 1753–1773. <https://doi.org/10.1175/bams-d-18-0180.1>.
- Bengtsson, L., Hodges, K.I. and Froude, L.S.R. (2005) Global observations and forecast skill. *Tellus A*, 57(4), 515–527. <https://doi.org/10.3402/tellusa.v57i4.14723>.
- Bi, L., Jung, J.A., Morgan, M.C. and Le Marshall, J.F. (2011) Assessment of assimilating ASCAT surface wind retrievals in the NCEP global data assimilation system. *Monthly Weather Review*, 139(11), 3405–3421. <https://doi.org/10.1175/2011MWR3391.1>.
- Bormann, N., Saarinen, S., Kelly, G. and Thépautet, J.-N. (2003) The spatial structure of observation errors in atmospheric motion vectors from geostationary satellite data. *Monthly Weather Review*, 131(4), 706–718. [https://doi.org/10.1175/1520-0493\(2003\)131](https://doi.org/10.1175/1520-0493(2003)131).
- Cress, A. (2020) "Validation and impact assessment of Aeolus observations in the DWD modeling system. Status report,". Aeolus NWP Impacts Working Meeting, Virtual. Available at: https://www.aeolus.esa.int/confluence/display/CALVAL/Aeolus+NWP+impact+working+meeting+2?preview=/12354328/12354463/5_DWD_acress_aeolus_20200617.pdf (Accessed November 15, 2020)
- Daley R. (1991) "Atmospheric Data Analysis. Cambridge University Press", Cambridge, 457 pp., ISBN-13978-0521458252.
- de Kloe, J. (2019) 'Aeolus L2B/L2C product handbook'. Technical report, ESA, REF: AE-TN-KNMI-GS-0185, internal document available for registered Aeolus Cal/Val teams.
- de Kloe, J. and Coauthors (2020) Aeolus data innovation science cluster DISC ADM-Aeolus level-2B/2C processor input/output data definitions Interface control document, Technical report, KNMI, Aeolus, DISC, REF: AED-SD-ECMWF-L2B-037. Available at: <https://earth.esa.int/eogateway/documents/20142/37627/Aeolus-L2B-2C-Input-Output-DD-ICD.pdf> (Accessed August 27, 2020).
- Garrett, K., Liu, H., Ide, K., Lukens, K. E., and Cucurull, L. (2020) 'Updates to Aeolus Impact Assessment on NOAA global NWP'. 2nd ESA Aeolus Cal/Val and Science Workshop, Virtual, Nov February 6, 2020. Available at: https://www.dropbox.com/s/cd0r1gz7t77gq0g/Kevin_Garrett_Oral_Evaluation_of_Aeolus.pptx?dl=0 (Accessed May 20, 2021).
- Hagelin, S., Azad, R., Lindsog, M., Schyberg, H. and Körnich, H. (2021) Evaluating the use of Aeolus satellite observations in the regional NWP model Harmonie-Arome. *Atmospheric Measurement Techniques*, 14, 5925–5938. <https://doi.org/10.5194/amt-14-5925-2021>.
- Hoffman, R.N., Kumar, K., Boukabara, S., Yang, F. and Atlas, R. (2018) Progress in forecast skill at three leading global operational NWP centers during 2015–17 as seen in summary assessment

- metrics (SAMs). *Weather of Forecasting*, 33, 1661–1679. <https://doi.org/10.1175/WAF-D-18-0117.1>.
- Hoffman, R.N., Lukens, K.E., Ide, K. and Garrett, K. (2022) A collocation study of atmospheric motion vectors (AMVs) compared to Aeolus wind profiles with a feature track correction (FTC) observation operator. *Quarterly Journal of the Royal Meteorological Society*, 148, 321–337. <https://doi.org/10.1002/qj.4207>.
- Hollingsworth, A. and Lonnberg, P. (1986) The statistical structure of short-range forecast errors as determined from radiosonde data. Part I: the wind field. *Tellus*, 38A(2), p111–p136. <https://doi.org/10.3402/tellusa.v38i2.11707>.
- Jung, J. and Coauthors (2016) ‘Development of advanced data assimilation techniques for improved use of satellite-derived atmospheric motion vectors’. Available at https://www.weather.gov/media/sti/nggps/09%20Jung_nggps_Aug_2016.pdf
- Kleist, D.T. and Coauthors. (2009) Introduction of the GSI into the NCEP global data assimilation system. *Weather of Forecasting*, 24, 1691–1705. <https://doi.org/10.1175/2009WAF2222201.1>.
- Kleist, D. T. and Coauthors (2021) ‘NCEP operational global data assimilation upgrades: from versions 15 through 16’. Special Symposium on Global and Mesoscale Models, Virtual, American Meteorological Society, 12.3. Available at: <https://ams.confex.com/ams/101ANNUAL/meetingapp.cgi/Paper/378554>.
- Liu, H., Garrett, K. Ide, K., Hoffman, R. N., and Lukens, K. E. (2020) ‘Bias correction and Error Specification of Aeolus Winds for NOAA Global Data Assimilation System’. 2nd ESA Aeolus CAL/VAL and Science Workshop, Nov February 6, 2020. Available at: https://www.dropbox.com/s/f518n7n8ouhgwhy/Hui_LIU_Flash_Evaluation_update.pdf?dl=0 (Accessed May 20, 2021).
- Liu, H., Garrett, K. Ide, K., Hoffman, R. N., and Lukens, K. E. (2022) ‘A Statistically Optimal Analysis of Systematic Differences in Winds from Aeolus Level-2B Data and the NOAA/FV3GFS’, Atmospheric Measurement Technique Discussion, <https://doi.org/10.5194/amt-2022-20>.
- Lukens, K.E., Ide, K., Garrett, K., Liu, H., Santek, D., Hoover, B. and Hoffman, R.N. (2022) Exploiting Aeolus L2B winds to better characterize atmospheric motion vector bias and uncertainty. *Atmospheric Measurement Techniques Aeolus Special Issue.*, 15, 2719–2743. <https://doi.org/10.5194/amt-2021-277>.
- National Academies of Sciences, Engineering, and Medicine. (2018) *Thriving on our Changing Planet: A Decadal Strategy for Earth Observation from Space*. The National Academies Press, Washington, D.C. <https://doi.org/10.17226/24938>.
- Reitebuch, O. (2012) ‘The Spaceborne Wind Lidar Mission ADM-Aeolus, in: *Atmospheric Physics: Background – Methods – Trends*. U., Springer, Berlin, Heidelberg, 815–827, https://doi.org/10.1007/978-3-642-30183-4_49.
- Reitebuch, O., Bracci, F., and Lux, O. (2020) ‘Assessment of the Aeolus performance and bias correction - results from the Aeolus DISC’. 2nd Aeolus Cal/Val Workshop. Available at: https://www.dropbox.com/s/m3kjp540otwm17/Oliver_Reitebuch_Oral_Assessment-Aeolus-DISC.pdf?dl=0 (Accessed May 20, 2021).
- Reitebuch, O. and Coauthors. (2009) ‘The airborne demonstrator for the direct-detection Doppler wind Lidar ALADIN on ADM-Aeolus’. Part I: instrument design and comparison to satellite instrument. *Journal of Atmosphere & Oceanic Technology*, 26, 2501–2515. <https://doi.org/10.1175/2009JTECHA1309.1>.
- Rennie, M., and Coauthors (2019) ‘First Results of the Impact of Aeolus Observations on ECMWF Forecasts,’ 1st ESA Aeolus Cal/Val and Science Workshop, March 25–29, 2019, Frascati, Italy.
- Rennie, M., Tan, D., Andersson, E., Poli, P., Dabas, A., de Kloe, J., Marseille, G.-J., and Stoffelen, A. (2020) ‘Aeolus Level-2B algorithm theoretical basis document’, Available at: <https://earth.esa.int/eogateway/documents/20142/37627/Aeolus-L2B-Algorithm-ATBD.pdf> (Accessed May 19, 2021)
- Rennie, M.P., Isaksen, L., Weiler, F., de Kloe, J., Kanitz, T. and Reitebuch, O. (2021) The impact of Aeolus wind retrievals on ECMWF global weather forecasts. *Quarterly Journal of the Royal Meteorological Society*, 147, 1–32. <https://doi.org/10.1002/qj.4142>.
- Stoffelen, A. and coauthors. (2005) The atmospheric dynamics Mission for global wind field measurement. *Bulletin of the American Meteorological Society*, 86(1), 73–87. <https://doi.org/10.1175/BAMS-86-1-73>.
- Straume, A.G., Rennie, M., Isaksen, L., De Kloe, J., Marseille, G.-C., Stoffelen, A., Flament, T., Stieglitz, H., Dabas, A., Huber, D., Reitebuch, O., Lemmerz, C., Lux, O., Marksteiner, U., Weiler, F., Witschas, B., Meringer, M., Schmidt, K., Nikolaus, I., Geiss, A., Flamant, P., Kanitz, T., Wernham, D., von Bismarck, J., Bley, D., Fehr, T., Floberghagen, R. and Parinello, T. (2020) ‘ESA’s space-based Doppler wind Lidar Mission Aeolus first wind and aerosol product assessment results. In: Liu, D., Wang, Y., Wu, Y., Gross, B. and Moshary, F. (Eds.) *EPJ Web of Conferences 237: 01007*. Oberpfaffenhofen, Germany. <https://doi.org/10.1051/epjconf/202023701007> Accessed May 19, 2021.
- Straume-Lindner, A. G. (2018) ‘Aeolus sensor and product description’. Technical Report, European Space Agency - European Space Research and Technology Centre, The Netherlands. REF: AE-SU-ESA-GS-000. Available at: <https://earth.esa.int/eogateway/documents/20142/37627/Aeolus-Sensor-and-Product-Description.pdf> (Accessed May 19, 2021).
- Wang, X. and Lei, T. (2014) GSI-based four-dimensional ensemble-Variational (4DEnsVar) data assimilation: formulation and single-resolution experiments with real data for NCEP global forecast system. *Monthly Weather Review*, 142, 3303–3325. <https://doi.org/10.1175/MWR-D-13-00303.1>.
- Weiler, F., Rennie, M., Kanitz, T., Isaksen, L., Checa, E., de Kloe, J. and Reitebuch, O. (2021) Correction of wind bias for the lidar on-board Aeolus using telescope temperatures. *Atmospheric Measurement Techniques*, 14, 7167–7185. <https://doi.org/10.5194/amt-14-7167-2021>.

How to cite this article: Garrett, K., Liu, H., Ide, K., Hoffman, R.N. & Lukens, K.E. (2022) Optimization and impact assessment of Aeolus HLOS wind assimilation in NOAA’s global forecast system. *Quarterly Journal of the Royal Meteorological Society*, 148(747), 2703–2716. Available from: <https://doi.org/10.1002/qj.4331>